Bioactive Materials 29 (2023) 1–15

Contents lists available at ScienceDirect

Bioactive Materials

journal homepage: www.keaipublishing.com/en/journals/bioactive-materials

A suture-free, shape self-adaptive and bioactive PEG-Lysozyme implant for Corneal stroma defect repair and rapid vision restoration

Hang Zhou [a,1], Shaohua Zhang [b,1], Miao Lei [a,1], Yixin Cai [a], Honglei Wang [a], Jianguo Sun [b,*], Jingyuan Cui [a,c], Changsheng Liu [a], Xue Qu [a,c,d,**]

[a] Key Laboratory for Ultrafine Materials of Ministry of Education, School of Material Science and Engineering, Frontiers Science Center for Materiobiology and Dynamic Chemistry, East China University of Science and Technology, Shanghai, 200237, China
[b] Eye Institute and Department of Ophthalmology, NHC Key Laboratory of Myopia (Fudan University), Key Laboratory of Myopia, Chinese Academy of Medical Sciences, Shanghai Key Laboratory of Visual Impairment and Restoration, Eye & ENT Hospital, Fudan University, Shanghai, 200031, China
[c] Wenzhou Institute of Shanghai University, Wenzhou, 325000, China
[d] Shanghai Frontier Science Center of Optogenetic Techniques for Cell Metabolism, Shanghai, 200237, China

ARTICLE INFO

Keywords:
Injective implant
Suture free
Shape self-adaptive
Intraocular pressure endurance
Foraging behavioral test

ABSTRACT

Corneal transplantation is a prevailing treatment to repair injured cornea and restore vision but faces the limitation of donor tissue shortage clinically. In addition, suturing-needed transplantation potentially causes postoperative complications. Herein, we design a PEG-Lysozyme injective hydrogel as a suture-free, shape self-adaptive, bioactive implant for corneal stroma defect repair. This implant experiences a sol-gel phase transition via an in situ amidation reaction between 4-arm-PEG-NHS and lysozyme. The physicochemical properties of PEG-Lysozyme can be tuned by the components ratio, which confers the implant mimetic corneal modulus and provides tissue adhesion to endure increased intraocular pressure. In vitro tests prove that the implant is beneficial to Human corneal epithelial cells growth and migration due to the bioactivity of lysozyme. Rabbit lamellar keratoplasty experiment demonstrates that the hydrogel can be filled into defect to form a shape-adaptive implant adhered to native stroma. The implant promotes epithelialization and stroma integrity, recovering the topology of injured cornea to normal. A newly established animal foraging behavior test prove a rapid visual restoration of rabbits when use implant in a suture free manner. In general, this work provides a promising preclinical practice by applicating a self-curing, shape self-adaptive and bioactive PEG-Lysozyme implant for suture-free stroma repair.

1. Introduction

Cornea is the outermost layer of the eye, and plays a crucial role in visual system [1]. In terms of physiological function, cornea not only protects the intraocular structure, but also refracts light to the retina to produce vision. The corneal injury resulted from trauma and infections is the second leading cause of blindness only to cataract [2]. The corneal stroma may partially degrade in severe and progressive cases of corneal stroma inflammation, compromising the structural integrity of cornea and damaging its visual function. Penetrating keratoplasty (PK) or anterior lamellar keratoplasty (ALK) to implant native corneal substitutes (e.g., human donor cornea, xenogeneic decellularized cornea) are efficient to treat corneal stroma defect and restore vision. However, the shortage of human donors and the high expenditure on transplantation surgery limit the application of this therapy, as a result, less than 5% of patients in the world receive treatment each year [3]. Meanwhile, xenogeneic decellularized corneal donors face the risk of the biosafety of sources and latent immunogenicity. It is urgent to develop artificial corneal implants to alleviate donor tissue shortage clinically.

The ideal artificial corneal implants should have physicochemical

Peer review under responsibility of KeAi Communications Co., Ltd.
* Corresponding author.
** Corresponding author. Key Laboratory for Ultrafine Materials of Ministry of Education, School of Material Science and Engineering, Frontiers Science Center for Materiobiology and Dynamic Chemistry, East China University of Science and Technology, Shanghai, 200237, China.
E-mail addresses: jgsun@fudan.edu.cn (J. Sun), quxue@ecust.edu.cn (X. Qu).
[1] These authors contributed equally to this work.

https://doi.org/10.1016/j.bioactmat.2023.05.008
Received 28 February 2023; Received in revised form 20 April 2023; Accepted 9 May 2023
Available online 28 June 2023
2452-199X/© 2023 The Authors. Publishing services by Elsevier B.V. on behalf of KeAi Communications Co. Ltd. This is an open access article under the CC BY-NC-ND license (http://creativecommons.org/licenses/by-nc-nd/4.0/).

properties similar to the native corneal tissue. For instance, high transmittance and low haze in the visible light range [4], high water content [5], similar modulus to native cornea [6], and three-dimensional geometries that match the shape of corneal defect precisely to restore the corneal thickness and refractive ability [7]. And also, the corneal implant should have appropriate biological functions to promote reconstruction of corneal epithelium and integration with the native corneal stroma [8]. In addition, adhesive implants are more promising than corneal implants requiring suture, since they can avoid suture-related complications including eye astigmatism [9], immune rejection [10], excretory bleeding at the suture site [11] and additional inflammation due to the prolonged operation time [12]. All these factors directly affect the corneal repair and the vision recovery in the future.

An attractive strategy is to develop a self-curing hydrogel with interfacial adhesion, shape self-adaption ability and bioactivity as artificial corneal implant. Hydrogel is a class of highly transmittable, highly water-content soft materials composed of polymer chains that can mimic physicochemical properties of native corneal stroma. Thus, hydrogel is a potential implant candidate for corneal stroma repair. Recently, researchers have synthesized a series of bioactive and injective hydrogel with biomacromolecules such as gelatin [13–15], collagen [16–21], hyaluronic acid [22], acellular matrix [23,24] for cornea repair. Although these reported materials have shown the ability to promote corneal epithelialization and stroma repair, reactions are often photo-initiated to achieve the in-situ gelation. Particularly, widely used ultraviolet light (UV)-initiated reactions are photochemically cytotoxic or detrimental to DNA in cornea and retina [5]. Even if the usage of visible light to cure implanted precursors is infeasible for patients with keratitis in clinic.

In addition, some artificial corneal implants fail to provide interfacial adhesion to native tissue, as thus cannot withstand the tension from postoperative intraocular pressure. To impart artificial corneal implants with tissue adhesion properties, photosensitive groups have been utilized to produce aldehyde groups in situ to chemically bind to the tissue surface. However, it still causes concerns about photo-toxicity towards ocular tissue [25]. Some other works have employed dopamine moieties to provide interfacial integrity function, while also introduced unwanted colors into the materials to interfere vision [26].

Multi-armed poly ethylene glycol (PEG) derivatives with N-hydroxy succinimide (NHS) ester groups at each terminal have a high reactivity with nucleophilic amine groups. They provide opportunities to yield hydrogels rapidly with functional macromolecules, and also provide an ideal linkage with tissue surface expose amine simultaneously. Previously, our group used lysozyme and 4-arm-PEG-NHS to form a self-curing two-component hydrogel as an injectable glue to seal tissue [27]. We unexpectedly found that this hydrogel material with an appropriate PEG/Lysozyme ratio can well promote the adhesion and proliferation of L929 fibroblast cells, which may be related to the peptide segments (66–68) of lysozyme that is analogous to the integrin binding RGD sequence [28]. And Lysozyme, as a component of tears, serves as a bioactive component for corneal implants, which may provide better biocompatibility on the eye's surface [29].

Inspired by the above findings, we propose a new strategy to repair corneal stroma defect by exploring PEG-Lysozyme hydrogel as suture-free, shape self-adaptive and bioactive implants. Scheme 1 (a) demonstrates the formation mechanism of PEG-Lysozyme implant. Precursor solutions of lysozyme and 4-arm-PEG-NHS are mixed and injected into the defect to yield a self-curing implant via amide bond formation between these two components. Scheme 1 (b) highlights multiple functions of the PEG-Lysozyme. First, the PEG-NHS component reacts with amino groups on the native stroma to provide a firm interfacial connection to cornea and avoid surgical suturing. Second, the 4-arm-PEG-NHS and lysozyme mixture has a suitable fluidity before curing, therefore can fill into the irregular defect and form a highly shape adaptive hydrogel implant. Third, Lysozyme, as a major component in the implant, provides RGD-like peptides that might promote HCECs migration and induce a rapid epithelialization over the PEG-Lysozyme implant.

A New Zealand white rabbit anterior lamellar keratoplasty is used to evaluate the efficacy of PEG-Lysozyme implant on cornea stroma repair. We create a novel intraocular pressure endurance index i.e. Corneal endothelial bending angles (CEBA) to evaluate the tissue integration ability of this suture-free implant more reliably. Moreover, we establish a vision restoration assessment for the first time based on a foraging behavioral test of the experimental animal after surgery, the index of

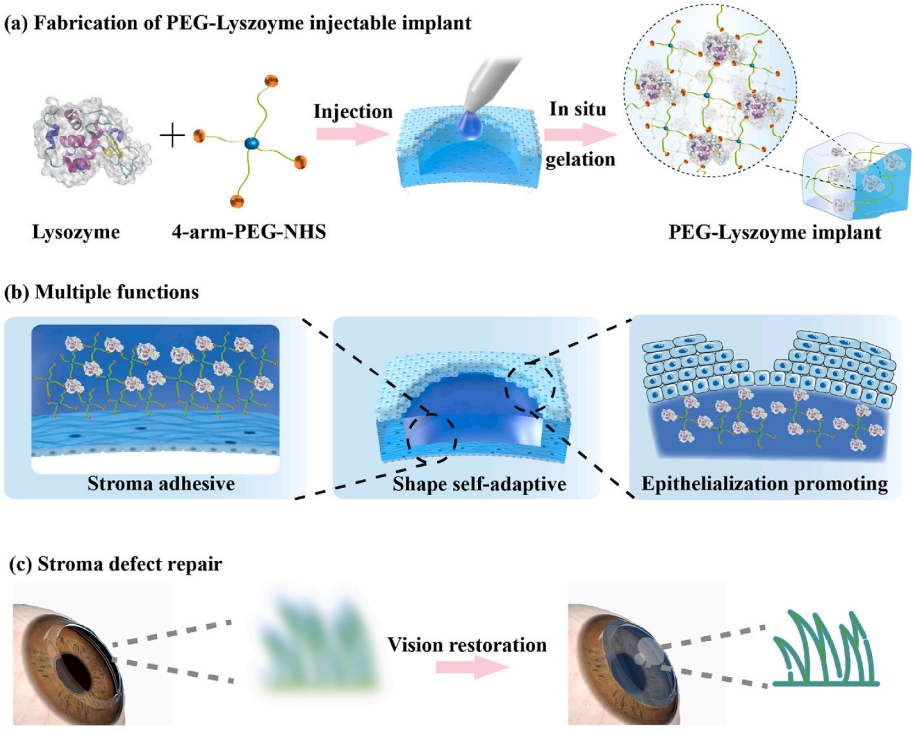

Scheme 1. The fabrication, functions and application of PEG-Lysozyme implant as artificial cornea substitute. (a) The PEG-Lysozyme implant is fabricated by injecting 4-arm-PEG-NHS and lysozyme precursors with an appropriate ratio and in situ curing via an amidation reaction between them. (b) The PEG-Lysozyme implant is endowed with multiple functions, including stroma adhesive, shape self-adaptive, epithelialization promotion. (c) PEG-Lysozyme implant can repair stroma defect and encourage rapid vision restoration.

which is critical to estimate the corneal function recovery under the intervention of biomaterials. Our work demonstrates PEG-Lysozyme injectable hydrogel functions as a suture free, shape self-adaptive and bioactive artificial corneal implant, which can promote corneal epithelialization and improve stromal construction, as thus represents a promising artificial corneal implant that might provide advanced surgical treatments for ocular clinical practice.

2. Material and methods

2.1. Materials

4-arm-poly (ethylene glycol) succinimidyl (4-arm-PEG-NHS, Mw = 10 kDa, Mw/Mn = 1.03) and 4-arm-PEG–NH_2–10k was purchased from SINOPEG, China. Hen egg-white lysozyme (20000 U mg^{-1}) was purchased from Beijing Solarbio Science & Technology Co. BCA assay kit was purchased from Beyotime. Sodium hyaluronate 0.1% eye drop solution (Hylo®) was purchased from URSAPHARM Arzneimittel GmbH (Germany). All cell culture-related reagents were purchased from Gibco (Gibco, USA). Cell counting kit-8 (CCK-8) was purchased from Dojindo (Japan). All other materials were purchased from Sigma-Aldrich unless otherwise specified.

2.2. Fabrication of PEG-Lysozyme implant

Phosphate buffer (PB) solution (0.1 M, pH = 7.5) and borax buffer solution (1 mg ml^{-1}, pH = 9.0) were prepared. Precursor A was prepared by dissolving lysozyme in borax buffer (150 mg ml^{-1}, 200 mg ml^{-1} and 225 mg ml^{-1}). Precursor B was prepared by dissolving 4-arm-PEG-NHS in PB buffer (150 mg ml^{-1}, 100 mg ml^{-1} and 75 mg ml^{-1}). PEG-Lysozyme implants were prepared in different ratios by mixing precursors A and B (PEG: lysozyme = 150:150 mg ml^{-1}; 100:200 mg ml^{-1}; 75:225 mg ml^{-1}). These implants were named P150-L150, P100-L200 and P75-L225.

2.3. Transmittance and haze

Mixed implant precursors (1 ml) were injected into the mold. After gelation, samples (2 cm in diameter, 3.2 mm in height) were removed from the mold, and three types of implants with different ratios were obtained. The transmittance (%) was measured by UV–visible spectrophotometer (Lambda 950, USA) at the wavelength of 350–800 nm and haze (%) was calculated by the transmittance. (The incident luminous flux is T_1. The total transmitted luminous flux through the sample is T_2. The instrument scattered luminous flux is T_3. The scattered luminous flux of instrument and sample is T_4.) The transmittance and haze is calculated as follows :

$$\text{Transmittance } (\%) = T_2/T_1 \times 100\%$$

$$\text{Haze } (\%) = [(T_4/T_2) - (T_3/T_1)] \times 100\%.\ (n = 6) \qquad \text{Equation 1}$$

2.4. Swelling ratio

Cylinder-shaped (10 mm diameter and 2 mm height) PEG-Lysozyme implants and native cornea with various solid contents were fabricated. The wet weight (W_0) of the implants was measured. Then samples were put into artificial tears (The main component is sodium hyaluronate) and incubated in a thermostatic shaker at 37 °C to achieve swelling balance. After 3 days, the weight (W_1) samples were measured after the water on the surface was removed. The swelling rate of implant is calculated as follows:

$$\text{Swelling ratio } (\%) = W_1/W_0 \times 100\%[30].\ (n = 3) \qquad \text{Equation 2}$$

2.5. Water content

After removing moisture on the surface of implants using filter paper, the samples were weighted (W_0). Then, the samples were freeze-dried and subsequently weighed (W_1). The water content in implants was calculated according to the formula:

$$\text{Water content } (\%) = (W_0–W_1)/W_0 \times 100\%[31].\ (n = 3) \qquad \text{Equation 3}$$

2.6. Measurement of gelation time

The gelation time was determined by the vial tilting method. We prepared implants with different ratios in sample vials at 37 °C, and the gelation time was recorded until there was no flow upon inverting the vial.

2.7. Rheological mechanics analysis

P150-L150, P100-L200 and P75-L225 implants were prepared into thin sheets (2 cm diameter and 1 mm thickness). The viscoelastic behaviors of implants were measured by a Thermo Haake MARS rheometer at 37 °C. During the measurement process, the amplitude sweep test was first performed to define the linear viscoelastic region (LVR) in which the storage modulus is independent of the strain amplitude. The amplitude in LVR was selected for oscillation frequency sweep tests within 0.1–10 Hz. The measured storage modulus (G′) represents the elastic properties of PEG-Lysozyme implants at this shear frequency, and the loss modulus (G″) represents viscous properties.

Besides, implant precursors were mixed and then injected into the testing plate immediately for oscillatory time-sweep measurements (strain 1%, frequency 1 Hz) conducted afterwards, which show the kinetics of reaction between PEG and lysozyme.

2.8. In vitro enzymatic degradation test

According to the above method, cylindrical P150-L150, P100-L200 and P75-L225 hydrogels with a radius of 10 mm and a height of 3 mm were prepared. In addition, lysozyme was replaced with 4-arm-PEG–NH_2–10k to prepare pure PEG hydrogels of the same size (4-arm-PEG–NH_2–10k:4-arm-PEG-NHS = 100 mg ml^{-1}:200 mg ml^{-1}) as the control group. After completely freeze-drying the sample, measure the mass (W_0). Place the sample in 2 ml of 0.5 mg ml^{-1} protease-K PBS solution and incubate at 37 °C for 3, 6, 12, 24, 48, and 72 h before freeze-drying to measure its weight (W_1).

$$\text{Residual mass} = W_1/W_0 \times 100\% \qquad \text{Equation 4}$$

2.9. In vitro adhesive strength test

Fresh porcine corneas were used to evaluate the tissue adhesion ability of PEG-Lysozyme implants. First, the corneal anterior lamellar of the porcine cornea was removed. Subsequently, two pieces of porcine corneas were fixed on the glass plate (2.5 cm × 7.5 cm) with cyanoacrylate implant (gold elephant 508) to overcome the curvature of the porcine corneas. Mixed implant precursors were injected into the gap between two pieces of the porcine cornea, which were then adhered together, known as a “sandwich” model. After 60 min, glass sheets were clamped and stretched by a mechanical stretching machine (SANS CMT2503) with a stretching rate 5 mm min^{-1}. The maximum value measured during the stretching process is the adhesive strength of the implant in the cornea. (n = 3)

2.10. In vitro assessment of hydrogel endurance in high intraocular pressure

Anterior lamellar keratoplasty was carried out on fresh porcine eyeballs with a 3 mm surgical trephine to create an injury (3 mm diameter and about 200 μm depth). The porcine eyes were divided into three groups, including the healthy cornea group, PEG-Lysozyme groups and No Implants group. The ocular perfusion was conducted by using an infusion system with a flow regulator and an infusion bottle filled with balanced salt solution (BSS, Alcon Laboratories, Inc.). A 30-gauge needle attached to the infusion system was entered into the peripheral anterior chamber at the corneoscleral limbus. The intraocular pressures were artificially elevated by controlling height of the infusion bottle. Intraocular pressure of 0 mmHg, 25 mmHg and 50 mmHg were applied respectively. Fourier-domain AS-OCT imaging system (RTVue, Optovue, Inc.) and Image J software were used to photograph and measure the bulge angle (The bulge angles of the endothelial layer under 0 mmHg and 50 mmHg intraocular pressure were α_0 and α_1, respectively) of the endothelial layer at the defect. Quantitative analysis was obtained according to the following formula:

$$\text{CEBA decrease (degree)} = \alpha_0\text{-}\alpha_1 \quad \text{Equation 5}$$

2.11. Released lysozyme

P150-L150, P100-L200 and P75-L225 implants were prepared according to the methods described above. The initial weight (W_0) of lysozyme is the weight of lysozyme in precursor solution. Then the samples were put into PBS solution and incubated in a thermostatic shaker at 37 °C for 1 day to achieve lysozyme releasing balance. The OD values of BCA standards at different concentrations were measured. And EXCEL was used to get the standard curve and standard equation ($Y = -0.6182X^3+1.1632X^2+1.0839X+0.0034$). The OD value of release lysozyme as X was substituted into the equation to calculate the concentration of lysozyme released. The concentration of lysozyme in PBS solution was measured by BCA assay kit, based on which the final weight (W_1) of lysozyme in PBS solution was calculated. Quantitative analysis was obtained according to the following formula:

$$\text{Release lysozyme} = W_1/W_0 \times 100\% \quad \text{Equation 6}$$

2.12. Cell culture

Human corneal epithelial cells (HCEC) and keratocytes were purchased from the American Type Culture Collection (ATCC,VA,USA). HCECs and keratocytes were used to evaluate the effects of three groups of PEG-Lysozyme implants on cell activity, and the cell attachment of PEG-protein implant. And the influence of PEG-Lysozyme implants on HCECs migration rate was studied. Experimentally, HCECs and keratocytes were evenly dispersed in DMEM medium containing 10% fetal bovine serum, penicillin (100 U ml^{-1}) and streptomycin (100 μg ml^{-1}). Then HCECs and keratocytes were put into the 37 °C cell incubator (5% CO_2) for cultivation.

2.13. Cell attachment on implants

To study the cell attachment characteristics of PEG-Lysozyme hydrogel, PEG-BSA was regarded as negative control group according to analogous methods. PEG-Lysozyme and PEG-BSA (PEG: protein = 100 mg ml^{-1}: 200 mg ml^{-1}) implants were fabricated in 24-well plates. After complete gelation, the HCECs and keratocytes were seeded on samples (5×10^4/well). After 12 h, the morphology of HCECs and keratocytes was observed by an inverted fluorescence microscope (DMi8 manual, Leica, Germany).

Next, we performed a cell attachment inhibition experiment. Specifically, HCECs and keratocytes were seeded on the substrate of PEG-Lysozyme implant in the condition of normal DMEM medium, serum free DMED medium, or medium containing antibodies against integrin β1 (Abcam, ab95623), integrin β3 (Abcam, ab210515) (1: 200 dilution in DMEM). The HCECs and keratocytes were seeded on samples (5×10^4/well) and cultured for 12 h. After cells were fixed in 4% paraformaldehyde solution for 15 min and rinsed twice with PBS solution. Then, samples were treated with Triton X-100 (0.1%, v/v) solution for 10 min to increase cell permeability. Besides, samples were blocked with BSA (5% (w/v) in PBS) solution for 60 min to shield non-specific protein adhesion sites on cell surface. And samples were then rinsed and incubated with the primary antibody for the focal adhesion protein vinculin (1: 200 dilution in 5% BSA), followed by incubating with Alexa Fluor 568 goat anti mouse IgG (1:500 dilution, in 5% BSA Molecular Probes) before a final rinse in PBS [28]. In addition, samples were attained with 5 μg ml^{-1} of FITC-phalloidin (45 min) and 5 μg ml^{-1} of DAPI (45 min) for cytoskeleton and nuclei staining, respectively. Cells were observed by confocal laser scanning microscopy (CLSM, Nikon, Japan). Cell average spreading area was evaluated by randomly photographing cells on ten places of different samples and calculated using Image J software. (n = 3)

2.14. Cell proliferation and 2D cell scratch test

1 ml PEG-Lysozyme implants precursor with three different ratios were injected into 24-well plate. After complete gelation, HCECs and keratocytes were seeded on samples and cell culture plate (5×10^4/well), maintained at 37 °C and 5% CO_2. After 1,3,5 days incubation, the cell morphologies were observed by an inverted microscope. The cell viability was evaluated by CCK-8 assays (DOJINDO) at 1,3 and 5 days post culture. The medium containing fetal bovine serum (FBS) was removed at each predetermined time, and a fresh medium containing 10% CCK-8 was added for 2 h of incubation. The incubation solution was then transferred to a 96-well plate, and the absorbance was measured using a microplate reader at 450 nm. The OD value of PEG-Lysozyme was OD_1 and the OD value of TCP and DMEM was OD_2 and OD_0The formula is as follows:

$$\text{cell viability (\%)} = (OD_1\text{-}OD_0)/(OD_2\text{-}OD_0) \times 100\% \quad \text{Equation 7}$$

After 48 h incubation, HCECs layers on the surface of the implants were scratched using 200 μl pipette tips. At 0, 2 and 3 days after the scratch, the healing of the scratch was observed with an inverted fluorescence microscope. The Image J plus was used to quantitatively analyze the scratch area of day 0, 2, and 3, where the area of HCECs migrating to the scratch area was A_1 and the area of the initial scratch area was A_0, and the cell migration area (%) on 2 and 3 days was calculated. (n = 3)

The formula is as follows:

$$\text{cell migration area (\%)} = (A_1/A_0) \times 100\% \quad \text{Equation 8}$$

2.15. Rabbit corneal surgeries

Adult New Zealand white rabbits were used in this study. The New Zealand white rabbits in the experiment were provided by the EYE and ENT Hospital of Fudan University. All procedures have been approved by the Animal Research Committee. The animal ethics approval number is IACUC-DWZX-2021-022. General anesthesia was performed by oxybuprocaine hydrochloride eye drops. Under sterile conditions, a surgical trephine (Suzhou Xiehe Medical Device Company) with a diameter of 3 mm was used to produce a defect with 200 μm by rotating the knob once. And lamellar keratectomy was performed at the same depth with a

45° corneal scalpel (Sharpoint, American). According to the defect diameter and depth, the volume of the defect can be calculated. The mixed solution of PEG and lysozyme was injected semi-quantitatively into the defect as experimental groups. And stroma defect treated with PEG-Lysozyme and two interrupted sutures were regarded as a negative control. The group without gel injection was used as the blank group. Both eyes of each rabbit have surgery in the same group. The number of rabbits for each group is 6, a total of 18 rabbits is used in animal experiments. The visual field of rabbit is close to 360°, due to their lateral positioning in the skull [32]. Therefore, the two eyes of one rabbit need to be treated in the same way.

At time points of 0, 3, 5, 14 and 90 days after operation, the ocular examination was performed by slit-lamp biomicroscopy under general anesthesia. The transmittance of cornea and implanted samples was observed. The corneal epithelial defects were visualized with 0.1% fluorescein sodium staining under cobalt blue light. For evaluation of the epithelial and stroma, AS-OCT scan images were obtained by AS-OCT system at 0, 3, 5, 14 and 90 days after the operation.

Rabbits were euthanized 90 days postoperatively. The eyeball was fixed with 4% (v/v) paraformaldehyde (PFA) overnight, and then the tissue was dehydrated, embedded and sliced. Then H&E staining was performed with hematoxylin and eosin Kit (Sigma Aldrich), and then samples were under observation. The α-SMA/DAPI, ZO-1/DAPI and Masson were stained according to operation steps, and observed by fluorescence microscope.

The foraging behaviors of rabbits in the P100-L200 group, P100-L200+Suture group, No Implants group and healthy rabbits were estimated 14 days after operation, to evaluate the degree of postoperative visual restoration. Before the experiment, animals were fed with special dried Timothy Hay for 3 days to build cognition, and then treated with hunger and thirst for 24 h. At the beginning of the experiment, in order to avoid rabbits using smell rather than vision to find food, the photos of Timothy Hay were used as false food, and the non food pictures were used as the interference group to test the time and road length of rabbits from the starting point to find the food pictures. (n = 6)

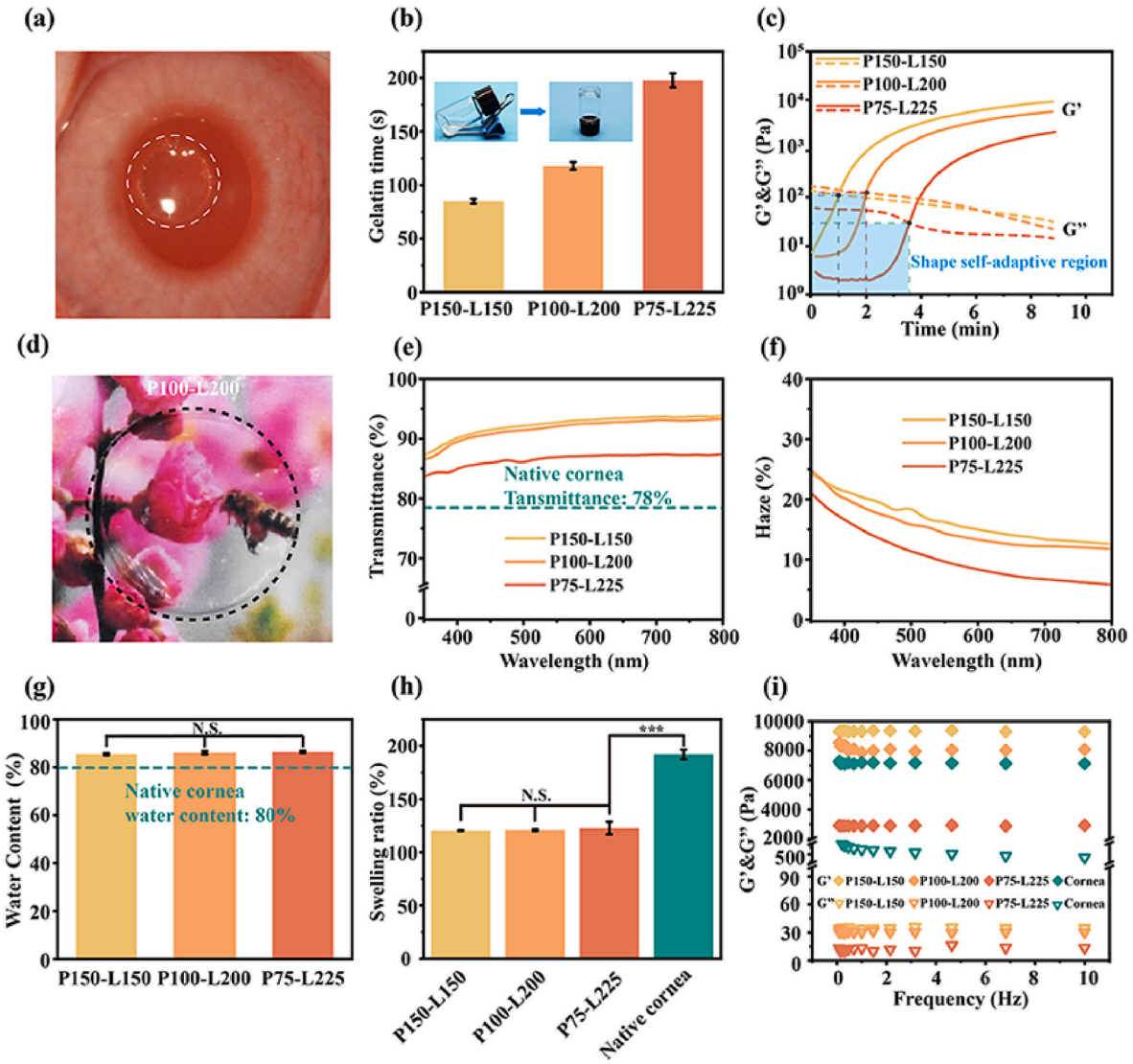

Fig. 1. In vitro characterization of PEG-Lysozyme implants. (a) Visual evidence indicates that the PEG-Lysozyme implant can be molded to defect shape in situ. (b) Gelation time, (c) dynamic time sweep curves, (d) macroscopic transparency, (e) transmittance, (f) haze, (g) water content, (h) swelling ratio, (i) dynamic frequency sweep curves of PEG-Lysozyme implants with different ratios. The results indicate PEG-Lysozyme has an appropriate gelation time about 1~3 min to form a shape self-adaptive implant with excellent optical properties, high water content, low swelling ratio, and adjustable modulus to meet the requirement of ocular implant. ($P > 0.05$ was considered to be statistically non-significant (N.S.); n = 3).

2.16. Statistical analysis

All data were expressed with mean standard deviation (SD) and analyzed using one-way ANOVA with post hoc tests. Significance was set at $p < 0.05$ (***$p < 0.001$, **$p < 0.01$, *$p < 0.05$), while $p > 0.05$ was considered to be statistically nonsignificant (N.S.).

3. Results and discussion

3.1. The gelation of PEG-Lysozyme implant and physicochemical characteristics

PEG-Lysozyme implant is fabricated by the amidation reaction of 4-arm-PEG-NHS and Lysozyme. Fig. 1 systematically evaluates the physicochemical performance of implants with different ratios of 4-arm-PEG-NHS to lysozyme. Specifically, the implant is named Px-Ly, where x refers to the mass concentration (w/v) of 4-arm-PEG-NHS in precursor A and y refers to the mass concentration of lysozyme in precursor B.

The prepolymer solution mixed with precursor A and B remained flowing for a while, allowing it to be injected easily and filled into defect rapidly to match the geometries. Subsequently, the implant experienced self-gelation to form a corneal implant. Fig. 1 (a) provides a visual evidence to indicate that the PEG-Lysozyme implant adapts to the shapes of defect on rabbit cornea and switches into a transparent gel. Gelation time of implants directly affects its shape adaptability and surgical operability. The gelation time is recorded when there is no flow upon inverting a vital containing the mixture of precursor solutions as shown in Fig. 1 (b). The gelation time of P150-L150, P100-L200, P75-L225 was measured as 85 ± 2.1 s, 118 ± 3.5 s, 198 ± 6.7 s respectively. Rheological oscillatory time-sweep measurements demonstrate that the increase of elastic modulus (G′, full line) of PEG-Lysozyme is time-dependent as shown in Fig. 1 (c). Within the 1–3 min after reaction begins, curves representing G′ in different groups intersected with the ones that representing the loss modulus (G″, dot line). The intersections suggest that the PEG and lysozyme mixture gelled at the corresponding time point, and this time point can also reflect the gelation time, which is consistent with the result of Fig. 1 (b). The shape self-adaptive region marked with light blue indicates that when G' < G″, the PEG-Lysozyme is in a flowing state favoring shape adaption to the defect site. Notably, PEG-Lysozyme has a suitable time window for implantation and curing.

PEG-Lysozyme implants with different ratios show high transparent appearances, as shown in Fig. 1 (d) and Fig. S1 (a). Quantitative transmittance and haze tests further prove the PEG-Lysozyme implants have high transmittance (close to 90%) and low haze (less than 25%) in the wavelength range of visible light, as shown in Fig. 1 (e-f). While the light transmittance of native corneal is 78% at 600 nm [30].

The water content of PEG-Lysozyme implants is more than that of native cornea (about 80% [33]), as shown in Fig. 1 (g). In addition, these implants show similar and less obvious swelling at about 120% when immersed in artificial tears, as shown in Fig. 1 (h) and Fig. S1 (b). The swelling ratio of native cornea is close to 200%. And the native cornea turns white after swelling. The cornea swelling can be related to the Donnan osmotic pressure stemming from proteoglycans of stroma [34]. And corneal stroma swelling increase interlamellar spacing resulting in light scattering and stroma whitening [35]. Finally, the rheological mechanical characteristics of PEG-Lysozyme implants with different ratios were explored, as shown in Fig. 1 (i). With the decrease of PEG and lysozyme ratio, the G′ of corresponding sample decreases. It is mainly because the shortage of 4-arm-PEG-NHS might reduce the crosslinking density of the resultant polymer network. Among them, the P100-L200 implant has a similar G' to native cornea (7150 ± 30 Pa) [36].

As shown in Fig. S2, PEG-Lysozyme implants can be degraded rapidly in 3 days, because protease-K can preferentially break the carboxyl terminal peptide bonds of sulfur-containing amino acids (cysteine, as one of the amino acids composed of lysozyme, is a sulfur-containing amino acid) to hydrolyze lysozyme into peptide segments [37]. However, PEG-PEG hydrogel is stable in protease-K solution due to the lack of active site for protease degradation, and it hardly degrades in 3 days. The results proved that the addition of lysozyme can not only endow the hydrogel with bio-activity, but also improve the biodegradability of PEG hydrogel in vivo.

Generally, these results in Fig. 1 indicate that the PEG-Lysozyme can be implanted by injection. Additionally, it provides appropriate gelation time to form a shape self-adaptive implant with excellent optical properties, high water content, low swelling ratio, and adjustable modulus to meet the requirement of ocular implant.

3.2. Corneal adhesion and intraocular pressure endurance of PEG-Lysozyme implants

The adhesion performance of PEG-Lysozyme implants on native stroma is evaluated by the lap-shear adhesion test. Experimentally, the epithelial layer of the fresh porcine cornea was firstly cut off. Then, two pieces of porcine corneas with the exposed stroma were adhered together by administration of the PEG-Lysozyme implant, and the adhesive strength of stromal layers was tested after the implant was in complete gelation, as shown in Fig. 2 (a). Fig. 2 (b) quantitatively shows the adhesive strength of PEG-Lysozyme implants with different ratios. The adhesive strength of P100-L200 (28.5 ± 1.4 kPa) is equivalent to that of P150-L150 (31.7 ± 2.1 kPa), which is significantly higher than that of P75-L225 (16 ± 3.6 kPa) and the fibrin glue (BeiXiu™, 14 ± 1.2 kPa). The adhesive strength of PEG-Lysozyme implant is weakened when the ratio of 4-am-PEG-NHS decreases in implant. It is presumably because the adhesion of PEG-Lysozyme implant on corneal stroma mainly depends on the formation of amide bond at the contacted interface, and the reduction of 4-arm-PEG-NHS ratio reduces the density of formed amide bonds.

In addition, one-third of patients suffer from elevated IOP (generally higher than 35 mmHg) after corneal transplantation due to increased anterior chamber fluid aqueous especially in glaucoma patients [38], and excessive IOP potentially leads to severe deformation of corneal implants and wounds cracking. PEG-Lysozyme with tunable storage modulus allows to mimic the stiffness of native corneal tissue. Therefore, PEG-Lysozyme implant may be able to withstand high IOP after implantation in the defect site. We employed an in vitro simulated intraocular pressure elevation model in Fig. 2 (c) to evaluate the IOP endurance of PEG-Lysozyme implants. Specifically, the anterior chamber of porcine eyeballs was infused with balanced salt solution to simulate different IOP conditions (Note: the simulated IOP can be converted according to the height of the bottle, 0.733 mmHg cm^{-1} [39]). PEG-Lysozyme implants with various ratios were applied to the corneal defect (diameter: 3 mm, depth: 300 μm) of fresh porcine eyeballs. After complete gelation, intraocular pressure was increased from 0 to 50 mmHg. The high intraocular pressure of patients usually as high as 21–50 mmHg (Human eye pressure ranges from 11 to 21 mmHg) [40–42]. Thus, IOP endurance of the hydrogel was investigated from 0 to 50 mmHg meeting clinical most needs.

The IOP endurance of implants in each group was semi-quantitatively evaluated according to the corneal endothelial bending angles (**CEBA**) that was calculated by AS-OCT images. The healthy cornea and defected cornea without implantation were set as positive and negative control groups, respectively. Fig. 2 (d) shows the CEBA in different groups under varying IOP. And Fig. 2 (e) summarized the quantitative CEBA decrease at the IOP 50 mmHg. The results indicate that with the increase of intraocular pressure, CEBA of healthy cornea remains at about 165° without significant decrease. And the CEBAs decrease in all PEG-Lysozyme groups show different level. The P150-L150 group (about 10 ± 2.3°) and P100-L200 group (about 8 ± 6.9°) have slightly lower CEBA decrease compared with that in P75-L225 implant treated group (about 14 ± 7.3°), and significantly lower CEBA decrease was found in the defected cornea with no implant protection (about 24 ± 3.5°). It indicates the application of PEG-Lysozyme

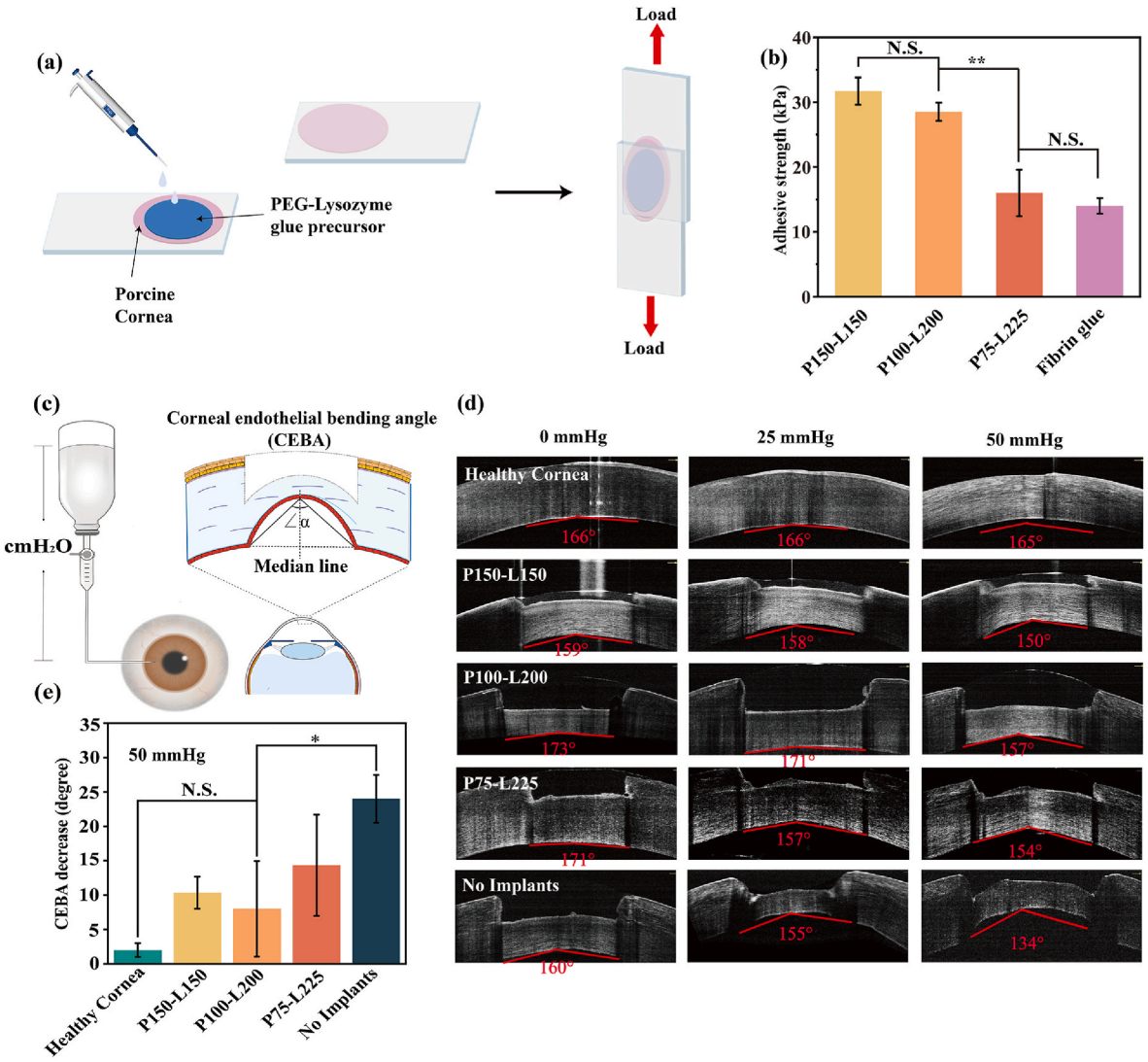

Fig. 2. In vitro adhesive performance of PEG-Lysozyme implants with different ratios using porcine cornea and eyeballs. (a) Schematic of the modified test for lap shear strength measurements and (b) average adhesive strengths of PEG-Lysozyme implants. (c) Schematic of ex vivo IOP endurance test, including an injection needle connected with the hanging bottle, an altimeter, and AS-OCT imaging system (AS-OCT). (d) AS-OCT imaging carried out in cadaveric porcine eyeballs under varying IOP. (f) Corneal endothelial bending angle (CEBA) decrease under 50 mmHg IOP. The results demonstrate PEG-Lysozyme implant provides tissue adhesion that allows suture-free implantation and endurance to high postoperative intraocular pressure. (*p < 0.05 and **p < 0.01; n = 3).

implants enables cornea stroma to withstand higher intraocular pressure, as thus avoid the deformation of postoperative cornea.

In short, the above results demonstrate that PEG-Lysozyme implant provides tissue adhesion that allows suture-free implantation into the defected corneal stroma [43]. In addition, the implant can endure high intraocular pressure and maintain the normal cornea, which potentially provide a stable mechanical environment favoring corneal stroma repair.

3.3. *In vitro biological evaluation of PEG-Lysozyme implants*

Corneal injury is usually accompanied by the apoptosis of corneal epithelial cells. Once corneal epithelium is damaged, the surrounding epithelial cells is recruited to the damaged area and reconstruct an epithelial layer [44,45]. Thus, the ideal corneal implants should be able to facilitate the migration of corneal epithelial cells rather than hinder [46]. Besides, keratocytes are important component of the corneal stroma layer. When the cornea stroma is damaged or inflamed, keratocytes are activated into fibroblasts and ultimately transformed into myofibroblasts, which can secrete collagen fibers and remodel the extracellular matrix [47–49]. So corneal implants should have cytocompatibility with keratocytes.

Specifically, HCECs and keratocytes were used to evaluate the cell adhesion, proliferation, and migration on PEG-Lysozyme implants. Fig. 3 (a) illustrates that lysozyme can promote cell attachment because its 66–68 peptide segments contain tripeptide DGR that is similar to RGD [50]. Fig. 3 (b) shows the cell morphology of HCECs and keratocytes cultured on different groups of hydrogel materials for 24 h. PEG-Lysozyme group was represented by P100-L200. PEG-BSA hydrogel is prepared by cross linking PEG-NHS individually with bovine serum albumin (BSA), and the material serve as control groups (Note: the PEG/BSA ratio is 100 and 200 mg ml^{-1}, the same as P100-L200). The results show that HCECs and keratocytes adhered to the surface of PEG-Lysozyme with a spreading morphology. However, HCECs and keratocytes accumulated on the concave area of PEG-BSA, and exhibited spherical shapes. These results indicate the special molecular structure of lysozyme is presumably responsible for good cell affinity in PEG-Lysozyme implant. To verify that lysozyme mediates cell adhesion via integrin, we performed cell attachment inhibition experiment. The integrin antibodies in cell DMEM medium can inhibits the attachment of

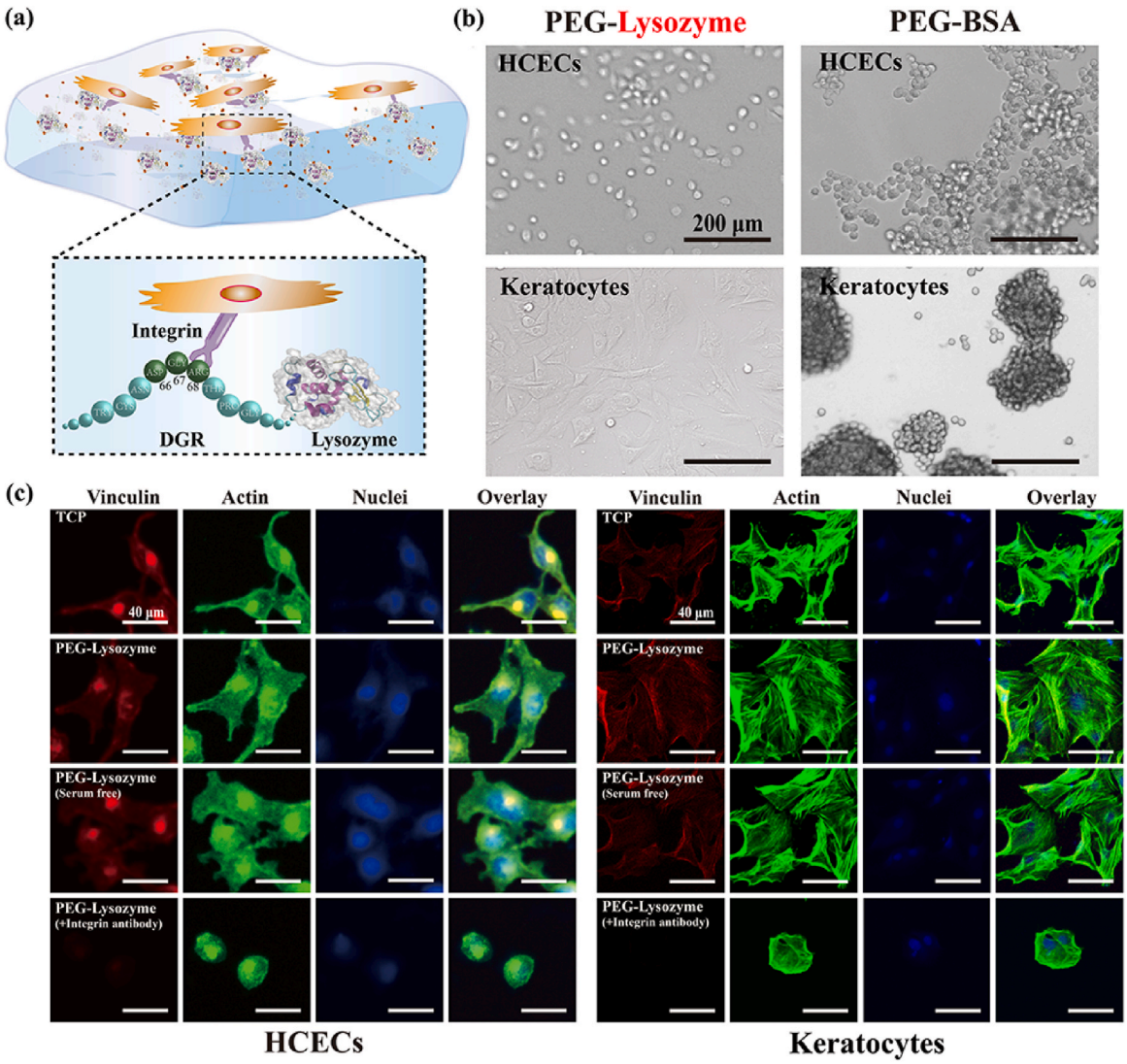

Fig. 3. Cell attachment study of PEG-Lysozyme implants. (a) The schematic illustrates that lysozyme has the ability to promote cell attachment because its peptide (66–68) contains tripeptide DGR. (b) Comparison of the spreading morphology of HCECs and keratocytes seeded on PEG-Lysozyme and PEG-BSA at 12 h post-seeding (scale bars, 200 μm). (c) Immunofluorescence staining of cells seeded on the surfaces of cell culture plate, PEG-Lysozyme, PEG-Lysozyme (serum free) and PEG-Lysozyme (+Integrin antibody) (scale bars, 40 μm). (n = 3).

cells. And immunofluorescence staining was performed to visualize actin cytoskeleton and integrin-mediated focal adhesion respectively. As shown in Fig. 3 (c), actin networks with significant outstretched filopodia extensions, lamellipodia protrusions (green) and pronounced focal adhesions (red) are observed in PEG-Lysozyme group. PEG-Lysozyme (serum free) group shows that serum has no effect on promoting cell attachment. However, under the action of integrin antibodies, the binding sites of integrin are blocked and the connection between cells and material surface is suppressed, thus the cell appears ellipsoidal with poorly defined stress fibers and focal adhesions. By calculating the average surface area of each cell, cells seeded on the PEG-Lysozyme in the normal medium adopted the highest average surface area similar to cell seeded on the culture plate in Fig. S3. The addition of integrin antibodies obviously reduces the average spread of cells on the PEG-Lysozyme surface. These results suggest that PEG-Lysozyme implant can provide cell adhesion sites to improve corneal repair.

The proliferation of HCECs and keratocytes was assessed by cell observation and CCK-8 assay respectively at the predetermined time points. HCECs and keratocytes cultured on PEG-Lysozyme with different ratios were compared. Fig. 4 (a) reveals the HCECs and keratocytes proliferated continuously on all the PEG-Lysozyme implants. The results of CCK-8 test in Fig. 4 (b) reveal that with the incubation time increasing, the cell viability on the PEG-Lysozyme hydrogel with three different component ratios are all close or over 100%, indicating the good biocompatibility of the materials and the P100-L200 and P75-L225 groups have comparable cell viability that is slightly higher than cell viability of P150-L150.

The migration of HCECs on PEG-Lysozyme implants with different ratios was investigated by an in vitro scratch test, as shown in Fig. 4 (c). HCECs seeded on PEG-Lysozyme implants show different migration rates, and the P100-L200 group shows the fastest migration rate and has filled the scratch area (about 600 μm width) at 3 days. Fig. 4 (d) quantifies the migration rate of HCECs on different substrates, the percentage of the cell migration areas (cells migrated to the scratched area accounted for the initial scratch area) at predetermined time points is calculated by Image J software. The results show that cell migration rate on the P100-L200 implant is significantly higher than on P150-L150 and P75-L225 implants after scratching, indicating that P100-L200 group facilitates HCECs movement.

Lysozyme is the critical component to endow implants with biological activity. However, the P75-L225 group with highest lysozyme ratio

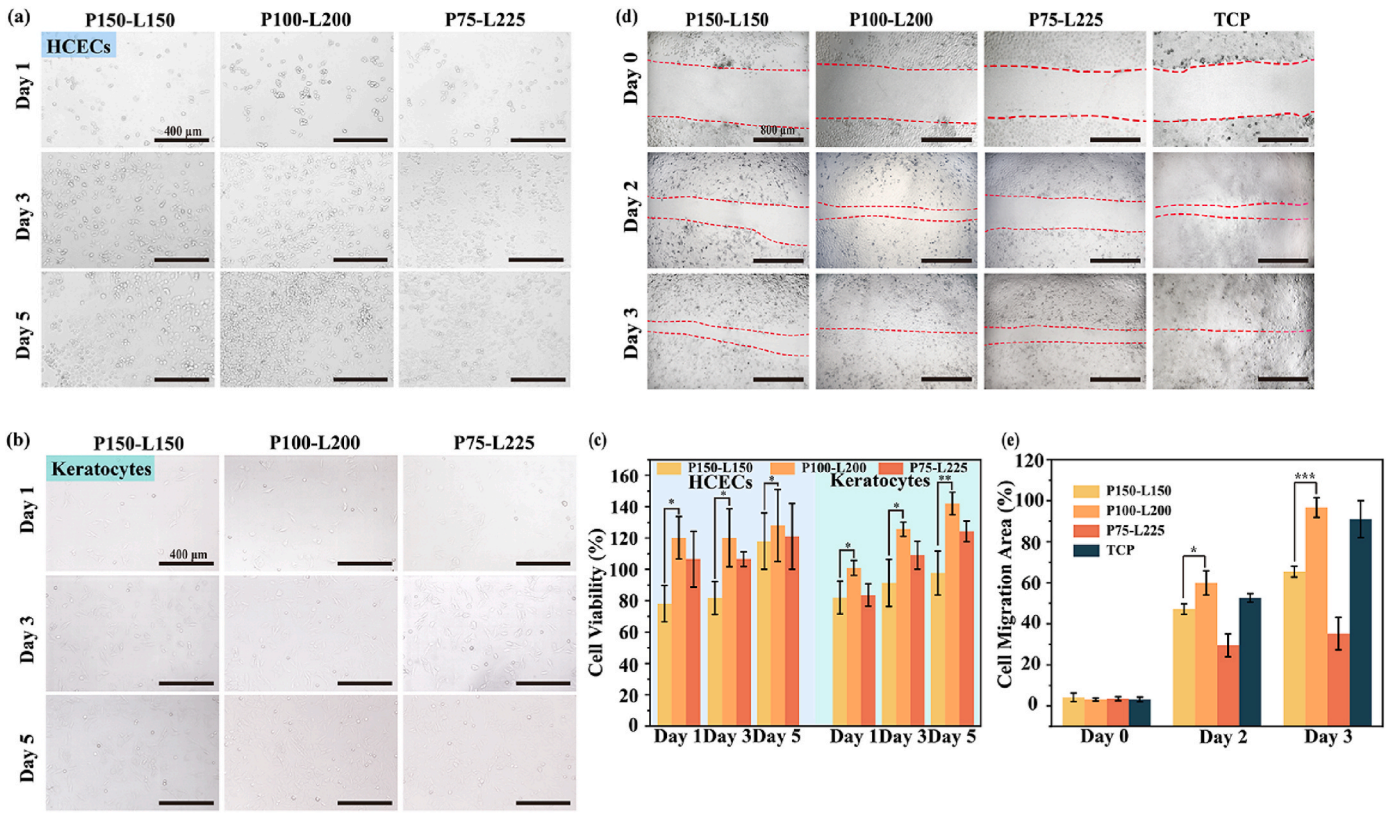

Fig. 4. In vitro biocompatibility and cell migration characterization of PEG-Lysozyme implants. (a) HCECs and (b) keratocytes proliferation on PEG-Lysozyme implants for different time (scale bars, 400 μm). (c) Quantification of HCECs and keratocytes cell viability on PEG-Lysozyme implants on day 1, day 3 and day 5 that was normalized by TCP data. (c) Scratch assay images of HCECs migration into the scratched area of PEG-Lysozyme implants at day 0, day 2 and day 3 (scale bars, 800 μm). (d) Quantification of cell migration area. (*$p < 0.05$ and ***$p < 0.001$; $n = 3$).

did not support the fastest cell migration compared to the P100-L200. This is presumably because the lower PEG in P75-L225 could not provide enough chemical cross-linking sites to bind all the lysozyme compared with P100-L200. As shown in Fig. S4, the lysozyme release (%) in the P225-L75 group is significantly higher than that in the P100-L200 group. Thus, the unbound lysozyme in P75-L225 is gradually released from the hydrogel, leading to the reduced bioactivity.

Overall, the results in Fig. 1 show the PEG-Lysozyme hydrogel with different ratios has similar transmittance, haze, water content and swelling ratio. Thus, the cell viability and cell migration speed are used as the parameters for selecting corneal implants. The results in Figs. 3 and 4 reveal that PEG-Lysozyme implants favor cells attachment, proliferation and migration. The P100-L200 group shows the best performances, so it is selected for the subsequent in vivo test.

3.4. *In vivo epithelialization and integrity of PEG-Lysozyme implant*

To further evaluate the potential of PEG-Lysozyme implant for repairing the defected cornea, in vivo studies were conducted by using a lamellar keratectomy corneal wound model. As illustrated in Fig. 5(a and b), an anterior lamellar corneal defect (3 mm diameter and about 200 μm depth) was created in New Zealand white rabbits, then P100-L200 implant was injected into the defect without suturing. To further elucidate the advantages of suture-free treatment supported by PEG-Lysozyme implant, a wound treated with PEG-Lysozyme implanting followed by two-point suturing was set as a control group, denoted as P100-L200+Suture. The wound without treatment was used as a negative control (in all group, $n = 6$).

Fig. 5 (c) shows the tissue response and epithelialization progress after different treatments. The regular optical and fluorescein staining of rabbits were performed by slit lamp at different time points within 90 days after operation. In the P100-L200 group, a clear boundary between implant and host tissue is observed at 0 day. After 3 days, the boundary became blurred and difficult to be clearly distinguished, which potentially suggests the integration between implants and tissues at the interface. In the long-term experiment, cornea treated with P100-L200 has kept clear, transparent and unvascularized. In contrast, in the P100-L200+Suture group, white ocular secretions are easily stranded on the suture point during the repairing process, which delayed the epithelialization. Besides, symptoms such as redness and edema appeared at the suture sites. And obvious neovascularization appeared near the suture in the P100-L200+Suture group at Day 90 of follow-up. In the No Implants group, no abnormal tissue response was observed and the cornea remained highly transparent, but the defect boundary of corneal stromal layer was still clearly observed at Day 14 postoperatively. Fluorescence images were taken under slit lamps with cobalt blue filters at different time points. The epithelial defects in green give information about the maturation of epithelialization in different groups. The results show that the size of corneal epithelial defect gradually decreases in all groups along time. At Day 5 postoperative, both the No Implants group and the P100-L200 group were completely epithelialized. While the P100-L200+Suture group did not complete epithelialized regeneration 14 days after operation. Interestingly, epithelial cells preferentially migrated from the non-sutured area to the defect center, referring the polarized fluorescent area in P100-L200+Suture group at Day 14, which implies that sutures may hinder epithelial migration and slow down the epithelialization. The quantitative epithelialization ratio in Fig. 5 (d) (calculated by comparing the area of green staining in corneal center with that at 0 day) further confirms that the epithelialization speed in P100-L200 group is faster than that in the P100-L200+Suture group. More details of the slit lamp in Fig. S5 show the smooth joint interface between the implant and the

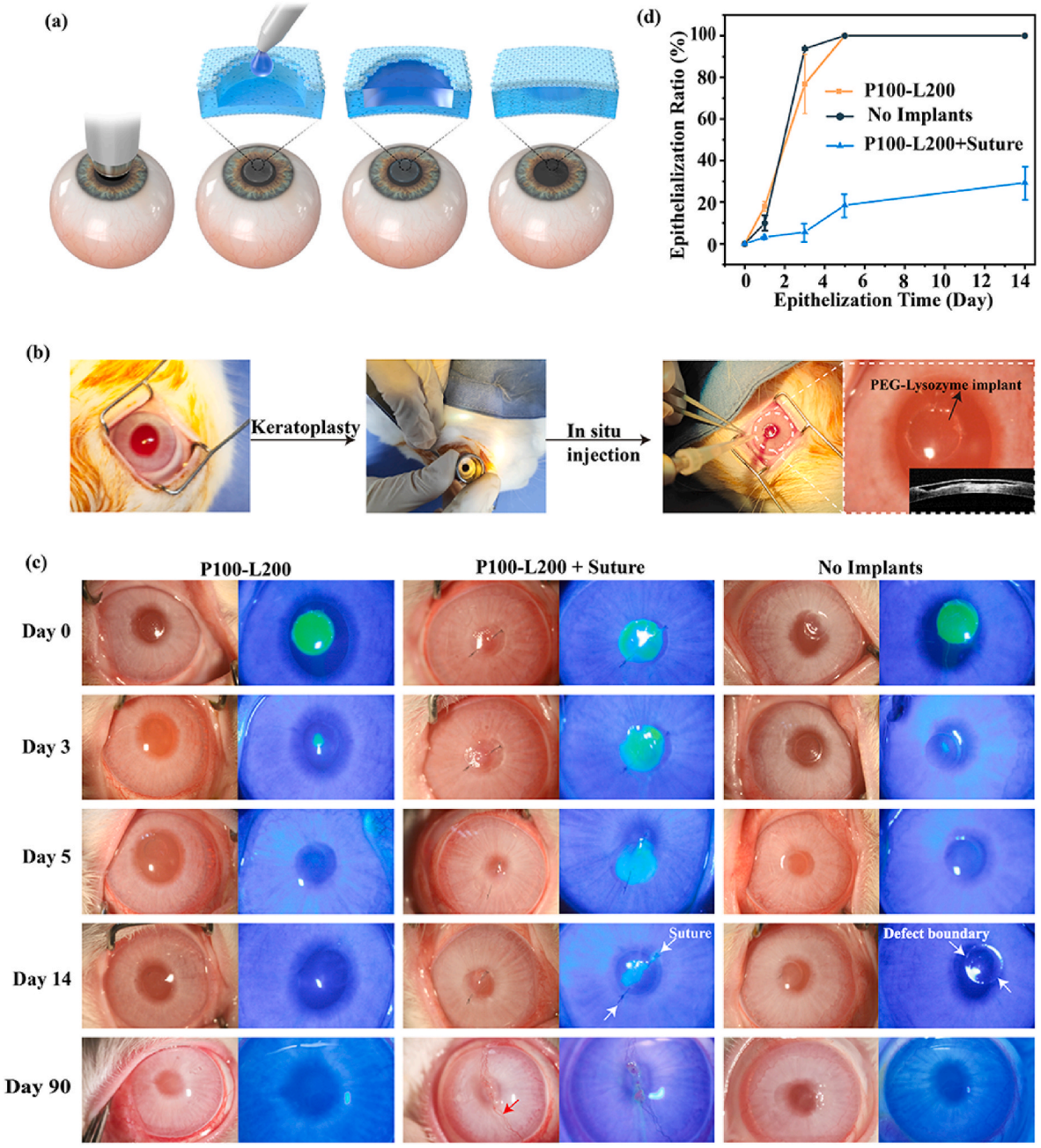

Fig. 5. The defect corneal epithelialization after in vivo application of P100-L200, P100-L200+Suture, and No Implants groups. (a) Scheme and (b) representative images for creating a corneal stromal defect with 200 μm in depth and 3 mm in diameter on rabbit eye. PEG-Lysozyme prepolymer solution was filled into corneal defect and match the shape of corneal defect precisely. (c) Representative slit lamp photographs and cobalt blue with fluorescein staining after in vivo application of P100-L200, P100-L200+Suture to rabbit cornea at different time points. (d) Epithelialization ratio analysis. The results imply that P100-L200 has the ability to promote cornea epithelialization, but the use of suture may hinder epithelial migration and slow down this process.

native cornea tissue in the P100-L200 group, while No Implants group still has obvious defect boundary at Day 14.

The cornea defects at different predetermined time points after surgery are recorded by the anterior segment optical coherence tomography (AS-OCT) in Fig. 6 (a). P100-L200 implant filled into the defect and adapted to the curvature of native tissue very well. Besides, a thin white tissue membrane was observed on the outer surface of the P100-L200 implant at Day 3 postoperatively (blue arrow marked) , which indicates the formation of the epithelium layer is consistent with the observation of fluorescence staining. The implanted materials are relatively intact in the initial stage (i.e., less than 14 days), and they gradually degrade with the prolonging implanted time. After 90 days surgery, implanted materials almost cannot be observed (marked with blue dotted box), and are replaced by the newly formed corneal stroma tissue. In contrast, the epithelialization degree in the P100-L200+Suture group was significantly lower than that of the P100-L200 group at the same time point. In the No implants group, the damaged corneal stroma was not restored to normal even at Day 90 (purple arrow marked).

The thickness recovery of defected cornea is evaluated by corneal topography after 90 days. Fig. 6 (b) shows the corneal topography maps of healthy cornea and the postoperative corneas with different treatments after 14 days and 90 days. The quantitative corneal central thickness after 90 days operation is summarized in Fig. 6 (c). A healthy rabbit cornea has a thickness about 470 μm. The defected cornea

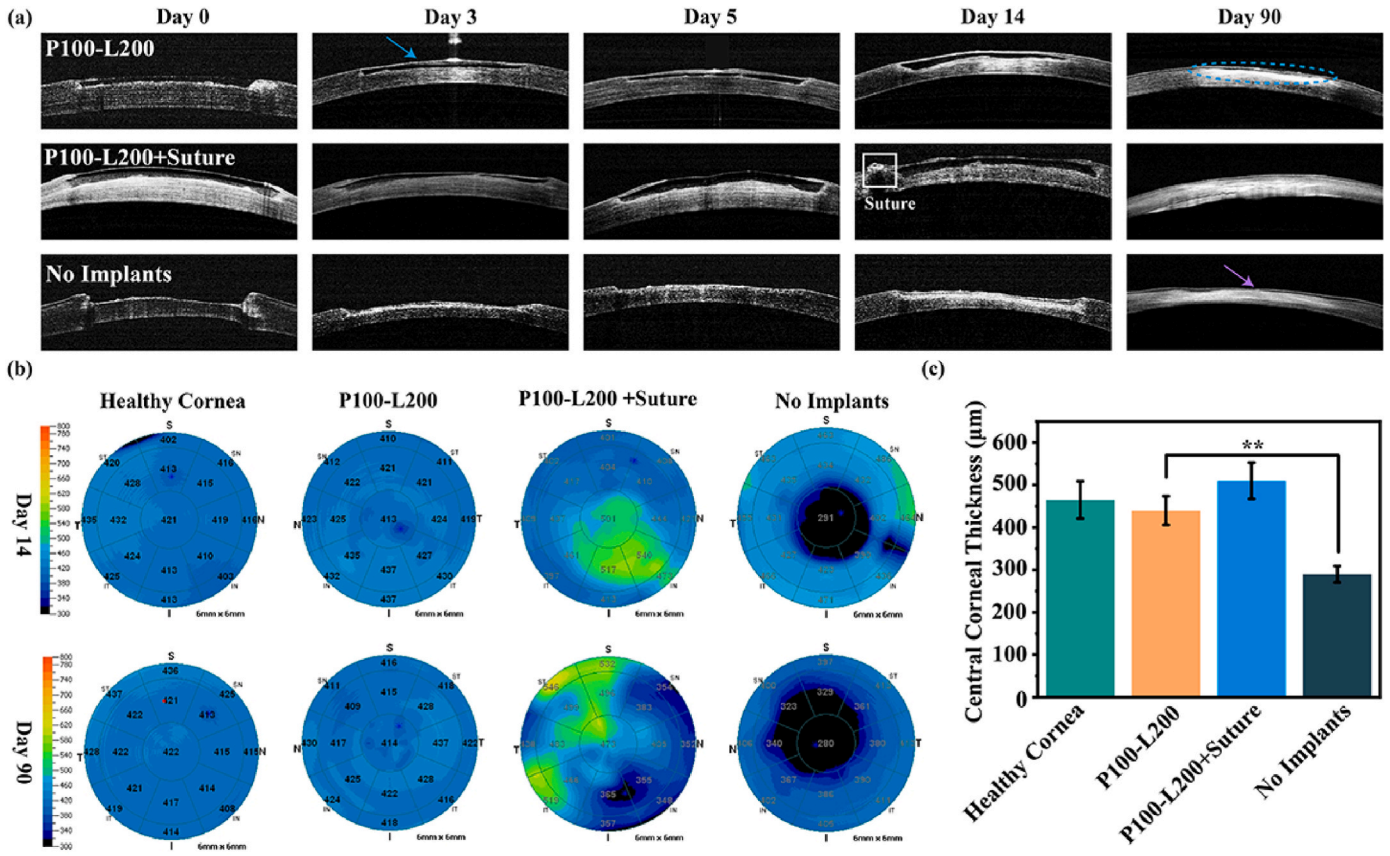

Fig. 6. (a) Anterior segment optical coherence tomography (AS-OCT) images and (b) corneal topography of P100-L200, P100-L200+Suture, No Implants groups. (c) Quantitative corneal thickness of different groups at 90 days post-operation. The P100-L200 shows the ability to quickly recover the thickness of injured cornea and promotes epithelialization after implantation. (**$p < 0.01$; $n = 6$).

intervened with implant materials basically recovered to the normal corneal thickness, which are 439 ± 34 μm for P100-L200 and 510 ± 43 μm for P100-L200+Suture group. And the control group without materials is about 290 ± 19 μm. The corneal topography of P100-L200+Suture group is not so smooth as the suture free group, and there are obvious protrusions in some areas, as indicated by the green color. The topographic maps of the postoperative cornea defect at different time points are shown in Fig. S6. In summary, the P100-L200 shows the ability to quickly recover the thickness of injured cornea and promotes epithelialization after implantation. And Fig. S7 shows that at day 14 after operation, P100-L200 group has basically repaired its thickness and curvature to provide refractive power and promote rapid vision restoration. The semi-quantitative injection and surface tension of hydrogel precursor solution may be the reason for maintaining adaptive thickness and curvature.

3.5. *In vivo histological evaluations and foraging behavior test*

Histological analysis based on immunofluorescence staining (ZO-1/DAPI and α-SMA/DAPI), Masson and hematoxylin eosin (H&E) staining of the cornea tissue specimens further supported the result of intraoperative observations (AS-OCT and slit-lamp biomicroscopy). ZO-1 is a tight junction protein in the epithelial monolayer [51]. Fig. S8 show short-term (14 days) tissue slice data. And Fig. 7 demonstrate long-term (90 days) cornea repair. Fig. 7 (a) shows that the epithelialization of P100-L200 group is multi-layered, which exhibits excellent tight junction ZO-1 (red) formation similar to that seen in normal corneal epithelium. The quantified fluorescence staining area shown in Fig. 7 (c) indicates with the treatment of P100-L200 implant, the expression of ZO-1 is comparable to health cornea. In contrast, the P100-L200+Suture group and No Implants group express a lower level of ZO-1.

α-SMA, known as α-smooth muscle actin, is stained to analyze the presence of myofibroblasts and corneal scarring. Persistent myofibroblast activity can lead to scarring fibrosis of the cornea. The second-row images in Fig. 7 (a) show that α-SMA is hardly expressed in P100-L200 and P100-L200+Suture groups, but slightly expressed in the No Implants group. The results suggest that P100-L200 might have low possibility to activate scar related cells.

H&E staining of corneal tissue samples further shows the recovery of corneal epithelia and stroma from Day 0 to Day 90. As shown in Fig. S9, P100-L200 (marked by blank arrow) is well integrated with cornea stroma at Day 0. Complete epithelialization in P100-L200 group was observed at Day 14. After 90 days implantation, the defect is observed to be almost completely occupied by new tissue. Masson staining in Fig. S10 also proved that a large amount of regenerated cornea stroma (circled by a red line) is observed at Day 90, and no material can be found any more. These results demonstrate the gradual degradation ability of P100-L200 and its improvement for corneal stroma regeneration and reepithelization.

The regenerated epithelial tissue is similar in shape and thickness to healthy cornea. In addition, there are no inflammatory cells or new blood vessels found in the P100-L200 implant, indicating a good ocular histocompatibility. Incomplete epithelialization was observed in the P100-L200+Suture group in Fig. S7 (b). The No Implants group failed to restore the normal corneal epithelial thickness, and the regenerated corneal epithelial layer is significantly thicker than that of healthy cornea (epithelial hyperplasia). Fig. 7 (d) and Fig. S7 (d) semi-quantitatively summarizes the thickness of regenerative epithelium in each group.

In order to evaluate the recovery of visual acuity in rabbits, the

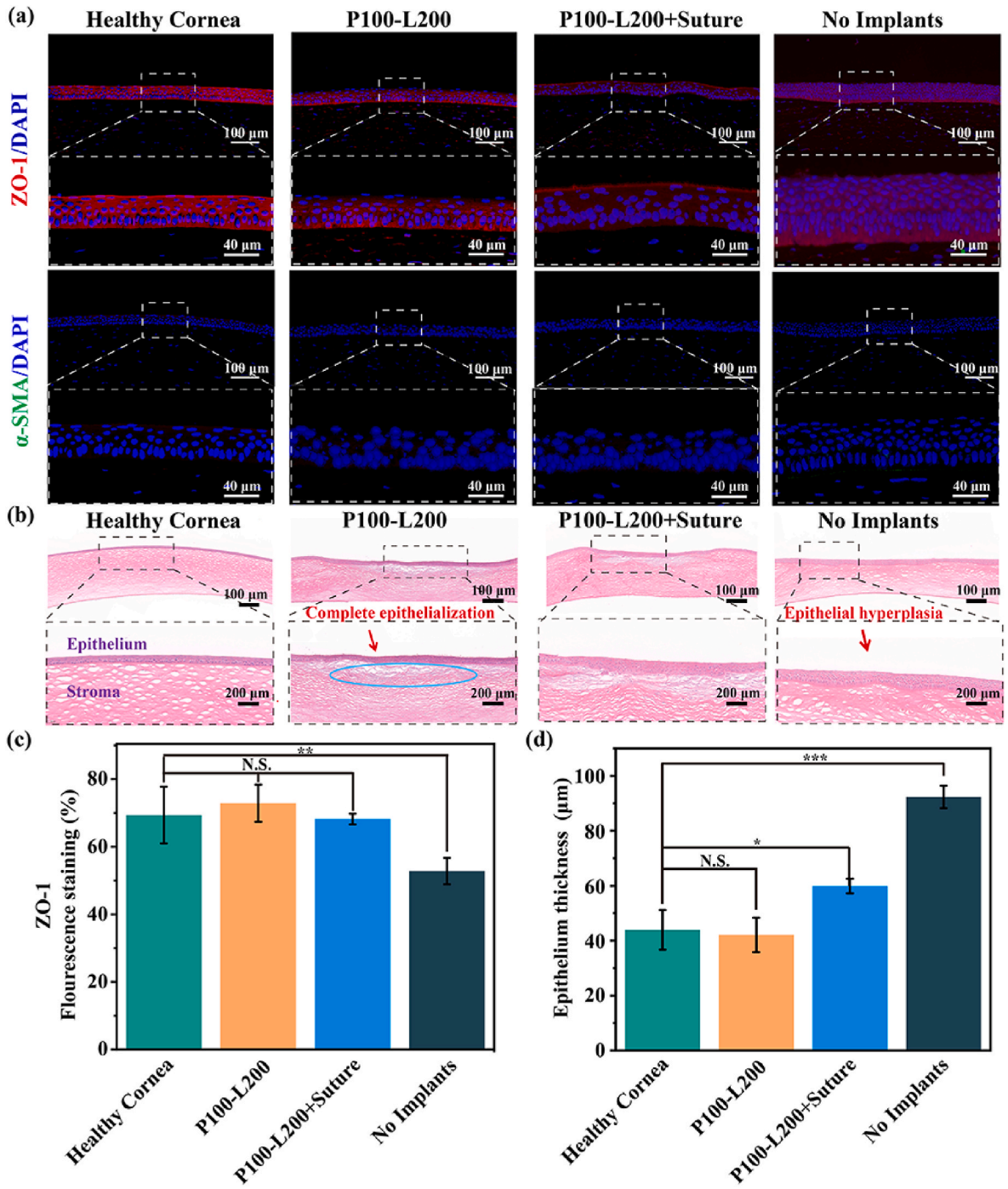

Fig. 7. Histological analysis of a rabbit corneal stromal defect at Day 90 post-operation. (a) Fluorescence staining images of smooth muscle actin (α-SMA) and tight junction protein (ZO-1) of cornea (scale bars, 40 μm and 100 μm). (b) H&E staining of healthy rabbit cornea and the injured rabbit cornea after different treatments 90 days after surgery (scale bars: 100 μm and 200 μm). (c) Quantitative fluorescence staining area of ZO-1 expression obtained from fluorescence staining images. (d) Thickness of epithelial layer for healthy cornea, P100-L200 and P100-L200+Suture treated, and untreated cornea obtained from histological images. (*$p < 0.05$, **$p < 0.01$ and ***$p < 0.001$; $n = 6$).

foraging behavioral test was performed. Fig. 8 (a) shows that before this test, animals were fed with special Timothy Hay for 3 days in advance to build cognition, and then treated with hunger and thirst for 24 h to construct addiction. The rabbit forages through the cooperation of vision and smell. And the blocking of olfactory sensation will not affect visual function [52,53]. Thus, the Timothy Hay photo was used as false food to eliminate the interference of food smell, and the non food photo was used as interference in the experiment. Although herbivore, such as rabbit and cattle, is farsighted and color blind, they can distinguish green grass within 3 m [54,55]. They were posted side by side on the wall of a confined space. All the animals started from a fixed starting point individually, and their foraging process was recorded. Exchanging the position of Timothy Hay photo and distraction photo to avoid rabbits accidently finding.

Fig. 8 (b) shows representative foraging images and paths of each group at the end of test, which indicate a fast food locating of the P100-L200 group and healthy group, while the animals in sham group and suture group are still in a confused search. Fig. 8 (c) and **(d)** reveal the

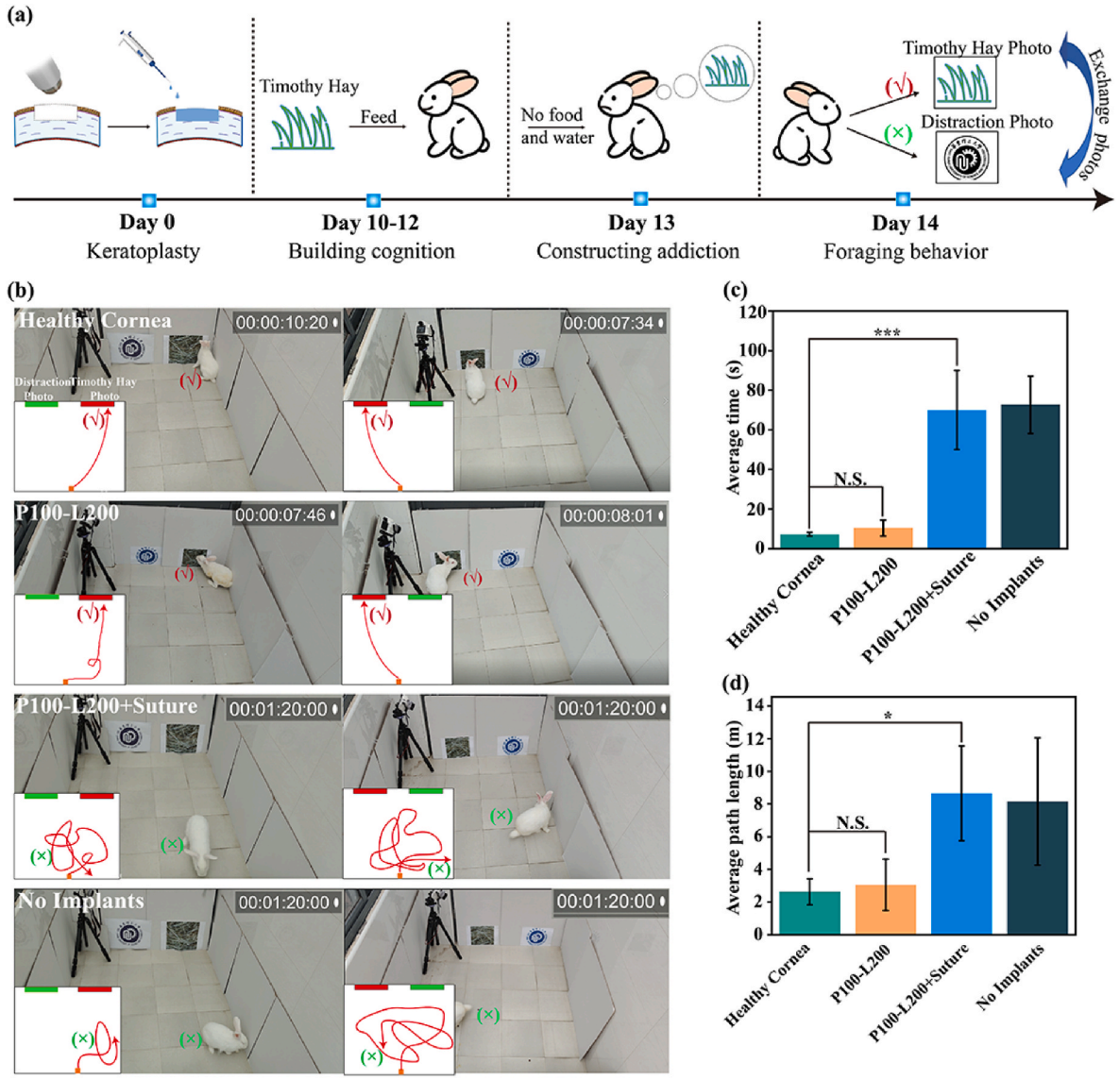

Fig. 8. Foraging behavior test of New Zealand white rabbits at day 14 after operation. (a) Before this test, animals were fed with special Timothy Hay for 3 days to build cognition and addiction, and then treated with hunger and thirst for 24 h. The Timothy Hay photo was used as false food to eliminate the interference of food smell, and the distraction photo was used as interference. And the parallel tests were also performed by changing the position of Timothy Hay photo and distraction photo to avoid rabbits accidently finding. The foraging behavior of the animals of different groups were recorded, (b) representative foraging image and paths (c) average time (d) average path length of successful foraging among groups including Healthy cornea, P100-L200, P100-L200+Suture, No Implants. The results reveal a more rapid foraging speed of P100-L200 group that can be comparable to the healthy group, implying a well postoperative visual acuity recovery was achieved by this suture-free and epithelialization promoted PEG-Lysozyme implant. (*$p < 0.05$ and ***$p < 0.001$; $n = 6$).

average time spent and average path length travelled when all the animals successfully find food photo, which provide quantitative evidence to indicate a more rapid foraging speed of P100-L200 group that can be comparable to the healthy group. This could be explained by the different central corneal thickness among groups at 14th post-surgery shown in Fig. 5 (d), where sham group still lack a large stroma tissue while suture group developed an excessive corneal thickness increase compared to the healthy cornea, both leading to abnormal refraction. The findings demonstrate the postoperative visual acuity recovery was well improved by this suture-free, epithelialization promoted and fit-to-shape PEG-Lysozyme implant. Rabbit behavior video can be obtained at Movie S1, Supporting Information.

4. Conclusion

In this study, we report a dual component implant containing 4-arm-PEG-NHS and lysozyme can be injected into the defected cornea to form a bioactive artificial cornea substitute for corneal stroma repair. Specifically, this implant experienced a sol-gel phase transition via an in situ amidation reaction when exposed to the cornea defect, as thus can self-adapt to the unregular defect very well. And also, the 4-arm-PEG-NHS component provided binding sites with the interfacial tissue, which enables the implant to firmly adhere to native stroma and realize a suture free treatment. In vitro intraocular pressure endurance test demonstrates that the implant can resist a high IOP and maintain the normal geometry of the damaged cornea. Moreover, the lysozyme component endows the implant with bioactivity. In vitro studies demonstrate that the implant exhibits good cell affinity, supporting the attachment, proliferation and migration of HCECs. An in vivo model of anterior lamellar keratoplasty in New Zealand rabbits further demonstrate that PEG-Lysozyme implant can promote rapid epithelialization and integrate well with the stroma with no obvious scarring or immune response.

Finally, the animal foraging behavior test demonstrates PEG-Lysozyme implant improved a postoperative visual acuity recovery compared to the suture group and no implant group. In all, our studies suggest PEG-Lysozyme is a very promising bioactive material for corneal stroma repair. Its injectability and suture-free characteristics may bring changes to the current ophthalmic surgery methods.

Ethics approval and consent to participate

All procedures have been approved by the Animal Research Committee. The animal ethics approval number is IACUC-DWZX-2021-022.

CRediT authorship contribution statement

Hang Zhou: Conceptualization, Data curation, Visualization, Investigation, Writing – original draft, Writing - review. **Shaohua Zhang:** Methodology. **Miao Lei:** Validation, Writing – review & editing. **Yixin Cai:** Writing – review & editing. **Honglei Wang:** Formal analysis. **Jianguo Sun:** Funding acquisition. **Jingyuan Cui:** Resources. **Changsheng Liu:** Funding acquisition. **Xue Qu:** Funding acquisition, Project administration.

Declaration of competing interest

Authors declare that they have no competing interests.

Acknowledgements

Support from the National Natural Science Foundation of China (31922041, 11932012, 32171341), National key research and development program (2021YFB3800800), the 111 project (B14018), the Science and Technology Innovation Project and Excellent Academic Leader Project of Shanghai Science and Technology Committee (21S31901500, 21XD1421100), the Scientific and Innovative Action Plan of Shanghai (No. 19441900600), the Natural Science Foundation of Shanghai (No. 19ZR1408300), the China Postdoctoral Science Foundation (D100-5R-22114), and the Shanghai Sailing Program (23YF1409700) are acknowledged.

Appendix A. Supplementary data

Supplementary data to this article can be found online at https://doi.org/10.1016/j.bioactmat.2023.05.008.

References

[1] X. Zhao, S. Li, X. Du, W. Li, Q. Wang, D. He, J. Yuan, Natural polymer-derived photocurable bioadhesive hydrogels for sutureless keratoplasty, Bioact. Mater. 8 (2022) 196–209.
[2] D.T.H. Tan, J.K.G. Dart, E.J. Holland, S. Kinoshita, Ophthalmology 3 corneal transplantation, Lancet 379 (9827) (2012) 1749–1761.
[3] P. Gain, R. Jullienne, Z. He, M. Aldossary, S. Acquart, F. Cognasse, G. Thuret, Global survey of corneal transplantation and eye banking, Jama Ophthalmol. 134 (2) (2016) 167–173.
[4] Z. Chen, J. You, X. Liu, S. Cooper, C. Hodge, G. Sutton, J.M. Crook, G.G. Wallace, Biomaterials for corneal bioengineering, Biomed. Mater. 13 (3) (2018).
[5] L. Li, C. Lu, L. Wang, M. Chen, J. White, X. Hao, K.M. McLean, H. Chen, T. C. Hughes, Gelatin-based photocurable hydrogels for corneal wound repair, ACS Appl. Mater. Interfaces 10 (16) (2018) 13283–13292.
[6] S. Molladavoodi, H.-J. Kwon, J. Medley, M. Gorbet, Human corneal epithelial cell response to substrate stiffness, Acta Biomater. 11 (2015) 324–332.
[7] D.W. DelMonte, T. Kim, Anatomy and physiology of the cornea, J. Cataract Refract. Surg. 37 (3) (2011) 588–598.
[8] X. Duan, C. McLaughlin, M. Griffith, H. Sheardown, Biofunctionalization of collagen for improved biological response: scaffolds for corneal tissue engineering, Biomaterials 28 (1) (2007) 78–88.
[9] C. Matossian, S. Makari, R. Potvin, Cataract surgery and methods of wound closure: a review, Clin. Ophthalmol. 9 (2015) 921–928.
[10] A.Z. Crawford, J.J. Meyer, D.V. Patel, S.E. Ormonde, C.N.J. McGhee, Complications related to sutures following penetrating and deep anterior lamellar keratoplasty, Clin. Exp. Ophthalmol. 44 (2) (2016) 142–143.
[11] C.G. Christo, J. van Rooij, A.J.M. Geerards, L. Remeijer, W.H. Beekhuis, Suture-related complications following keratoplasty - a 5-year retrospective study, Cornea 20 (8) (2001) 816–819.
[12] C. Cursiefen, K. Maruyama, D.G. Jackson, J.W. Streilein, F.E. Kruse, Time course of angiogenesis and lymphangiogenesis after brief corneal inflammation, Cornea 25 (4) (2006) 443–447.
[13] M. Rizwan, G.S.L. Peh, H.-P. Ang, N.C. Lwin, K. Adnan, J.S. Mehta, W.S. Tan, E.K. F. Yim, Sequentially-crosslinked bioactive hydrogels as nano-patterned substrates with customizable stiffness and degradation for corneal tissue engineering applications, Biomaterials 120 (2017) 139–154.
[14] E.S. Sani, A. Kheirkhah, D. Rana, Z. Sun, W. Foulsham, A. Sheikhi, A. Khademhosseini, R. Dana, N. Annabi, Sutureless repair of corneal injuries using naturally derived bioadhesive hydrogels, Sci. Adv. 5 (3) (2019).
[15] Y. Zhang, C. Li, Q. Zhu, R. Liang, C. Xie, S. Zhang, Y. Hong, H. Ouyang, A long-term retaining molecular coating for corneal regeneration, Bioact. Mater. 6 (12) (2021) 4447–4454.
[16] G.M. Fernandes-Cunha, K.M. Chen, F. Chen, P. Le, J.H. Han, L.A. Mahajan, H. J. Lee, K.S. Na, D. Myung, In situ-forming collagen hydrogel crosslinked via multi-functional PEG as a matrix therapy for corneal defects, Sci. Rep. 10 (1) (2020).
[17] C.D. McTiernan, F.C. Simpson, M. Haagdorens, C. Samarawickrama, D. Hunter, O. Buznyk, P. Fagerholm, M.K. Ljunggren, P. Lewis, I. Pintelon, D. Olsen, E. Edin, M. Groleau, B.D. Allan, M. Griffith, LiQD Cornea, Pro-regeneration collagen mimetics as patches and alternatives to corneal transplantation, Sci. Adv. 6 (25) (2020).
[18] X. Zhao, W. Song, Y. Chen, S. Liu, L. Ren, Collagen-based materials combined with microRNA for repairing cornea wounds and inhibiting scar formation, Biomater. Sci. 7 (1) (2019) 51–62.
[19] Y. Xu, J. Liu, W. Song, Q. Wang, X. Sun, Q. Zhao, Y. Huang, H. Li, Y. Peng, J. Yuan, B. Ji, L. Ren, Biomimetic convex implant for corneal regeneration through 3D printing, Adv. Sci. 10 (11) (2023) 16.
[20] W. Liu, C. Deng, C.R. McLaughlin, P. Fagerholm, N.S. Lagali, B. Heyne, J. C. Scaiano, M.A. Watsky, Y. Kato, R. Munger, N. Shinozaki, F. Li, M. Griffith, Collagen-phosphorylcholine interpenetrating network hydrogels as corneal substitutes, Biomaterials 30 (8) (2009) 1551–1559.
[21] W. Liu, K. Merrett, M. Griffith, P. Fagerholm, S. Dravida, B. Heyne, J.C. Scaiano, M. A. Watsky, N. Shinozaki, N. Lagali, R. Munger, F. Li, Recombinant human collagen for tissue engineered corneal substitutes, Biomaterials 29 (9) (2008) 1147–1158.
[22] F. Chen, P. Le, G.M. Fernandes-Cunha, S.C. Heilshorn, D. Myung, Bio-orthogonally crosslinked hyaluronate-collagen hydrogel for suture-free corneal defect repair, Biomaterials (2020) 255.
[23] F. Wang, W. Shi, H. Li, H. Wang, D. Sun, L. Zhao, L. Yang, T. Liu, Q. Zhou, L. Xie, Decellularized porcine cornea-derived hydrogels for the regeneration of epithelium and stroma in focal corneal defects, Ocul. Surf. 18 (4) (2020) 748–760.
[24] G. Yazdanpanah, X. Shen, T. Nguyen, K.N. Anwar, O. Jeon, Y. Jiang, M. Pachenari, Y. Pan, T. Shokuhfar, M.I. Rosenblatt, E. Alsberg, A.R. Djalilian, A light-curable and tunable extracellular matrix hydrogel for in situ suture-free corneal repair, Adv. Funct. Mater. 32 (24) (2022).
[25] G. Wollensak, E. Sporl, F. Reber, L. Pillunat, R. Funk, Corneal endothelial cytotoxicity of riboflavin/UVA treatment in vitro, Ophthalmic Res. 35 (6) (2003) 324–328.
[26] L. Koivusalo, M. Kauppila, S. Samanta, V.S. Parihar, T. Ilmarinen, S. Miettinen, O. P. Oommen, H. Skottman, Tissue adhesive hyaluronic acid hydrogels for sutureless stem cell delivery and regeneration of corneal epithelium and stroma, Biomaterials 225 (2019).
[27] H. Tan, D. Jin, X. Qu, H. Liu, X. Chen, M. Yin, C. Liu, A PEG-Lysozyme hydrogel harvests multiple functions as a fit-to-shape tissue sealant for internal-use of body, Biomaterials 192 (2019) 392–404.
[28] N.P. Reynolds, M. Charnley, R. Mezzenga, P.G. Hartley, Engineered lysozyme amyloid fibril networks support cellular growth and spreading, Biomacromolecules 15 (2) (2014) 599–608.
[29] D.S. Selinger, R.C. Selinger, W.P. Reed, Resistance to infection of the external eye: the role of tears, Surv. Ophthalmol. 24 (1) (1979) 33–38.
[30] M. Rafat, F. Li, P. Fagerholm, N.S. Lagali, M.A. Watsky, R. Munger, T. Matsuura, M. Griffith, PEG-stabilized carbodiimide crosslinked collagen-chitosan hydrogels for corneal tissue engineering, Biomaterials 29 (29) (2008) 3960–3972.
[31] H. Fan, J. Wang, Z. Jin, Tough, swelling-resistant, self-healing, and adhesive dual-cross-linked hydrogels based on polymer-tannic acid multiple hydrogen bonds, Macromolecules 51 (5) (2018) 1696–1705.
[32] M.W. Van Hof, I.S. Russell, Binocular vision in the rabbit, Physiol. Behav. 19 (1) (1977) 121–128.
[33] Y. Liang, W. Liu, B. Han, C. Yang, Q. Ma, W. Zhao, M. Rong, H. Li, Fabrication and characters of a corneal endothelial cells scaffold based on chitosan, J. Mater. Sci. Mater. Med. 22 (1) (2011) 175–183.
[34] M.R. Bryant, P.J. McDonnell, A triphasic analysis of corneal swelling and hydration control, J. Biomech. Eng. 120 (3) (1998) 370–381.
[35] J.W. Ruberti, A.S. Roy, C.J. Roberts, Corneal biomechanics and biomaterials, in: M. L. Yarmush, J.S. Duncan, M.L. Gray (Eds.), Annual Review of Biomedical Engineering, Vol vol. 132011, pp. 269-295.
[36] H. Hatami-Marbini, Viscoelastic shear properties of the corneal stroma, J. Biomech. 47 (3) (2014) 723–728.
[37] A.L.L. East, On the hydrolysis mechanisms of amides and peptides, Int. J. Chem. Kinet. 50 (10) (2018) 705–709.
[38] B.d.P.S. Bezerra, E. Chan, R. Chakrabarti, R.B. Vajpayee, Intraocular pressure measurement after corneal transplantation, Surv. Ophthalmol. 64 (5) (2019) 639–646.

[39] A. Esrafili, A. Wagner, S. Inamdar, A.P. Acharya, Covalent organic frameworks for biomedical applications, Adv. Healthc. Mater. 10 (6) (2021).
[40] Q. Zhang, Q. Tang, Y. Yang, J. Yi, W. Wei, Y. Hong, X. Zhang, F. Zhou, X. Yao, H. Ouyang, Wound dressing gel with resisted bacterial penetration and enhanced re-epithelization for corneal epithelial-stromal regeneration, Appl. Mater. Today 24 (2021).
[41] M. Baltaziak, H.F. Chew, D.W. Podbielski, I.I.K. Ahmed, Glaucoma after corneal replacement, Surv. Ophthalmol. 63 (2) (2018) 135–148.
[42] N. Yildirim, H. Gursoy, A. Sahin, A. Ozer, E. Colak, Glaucoma after penetrating keratoplasty: incidence, risk factors, and management, J. Ophthalmol. 2011 (2011).
[43] A.R. Irvine, H.E. Kaufman, Intraolar pressure following penetrating keratoplasty, Am. J. Ophthalmol. 68 (5) (1969) 835–844.
[44] R.A. Thoft, J. Friend, The X, Y, Z hypothesis of corneal epithelial maintenance, Investig. Ophthalmol. Vis. Sci. 24 (10) (1983) 1442–1443.
[45] A.V. Ljubimov, M. Saghizadeh, Progress in corneal wound healing, Prog. Retin. Eye Res. 49 (2015) 17–45.
[46] S.B. Anderson, R.F. de Souza, C. Hofmann-Rummelt, B. Seitz, Corneal calcification after amniotic membrane transplantation, Br. J. Ophthalmol. 87 (5) (2003) 587–591.
[47] M. Koulikovska, M. Rafat, G. Petrovski, Z. Vereb, S. Akhtar, P. Fagerholm, N. Lagali, Enhanced regeneration of corneal tissue via a bioengineered collagen construct implanted by a nondisruptive surgical technique, Tissue Eng. 21 (5–6) (2015) 1116–1130.
[48] B. Kong, L. Sun, R. Liu, Y. Chen, Y. Shang, H. Tan, Y. Zhao, L. Sun, Recombinant human collagen hydrogels with hierarchically ordered microstructures for corneal stroma regeneration, Chem. Eng. J. 428 (2022).
[49] B. Kong, Y. Chen, R. Liu, X. Liu, C. Liu, Z. Shao, L. Xiong, X. Liu, W. Sun, S. Mi, Fiber reinforced GelMA hydrogel to induce the regeneration of corneal stroma, Nat. Commun. 11 (1) (2020).
[50] T. Wu, Q. Jiang, D. Wu, Y. Hu, S. Chen, T. Ding, X. Ye, D. Liu, J. Chen, What is new in lysozyme research and its application in food industry? A review, Food Chem. 274 (2019) 698–709.
[51] H. Zhu, S. Parvinian, C. Preston, O. Vaaland, Z. Ruan, L. Hu, Transparent nanopaper with tailored optical properties, Nanoscale 5 (9) (2013) 3787–3792.
[52] A. Arshamian, J.K. Olofsson, F.U. Jonsson, M. Larsson, Sniff your way to clarity: the case of olfactory imagery, Chemosens. Percep. 1 (4) (2008) 242–246.
[53] L. Arteaga, A. Bautista, D. Gonzalez, R. Hudson, Smell, Survive Suck, Chemical Signals and Suckling in the Rabbit, Cat, and Dog, 12th Meeting of the Chemical Signals in Vertebrates, Leibniz Inst Zoo & Wildlife Res, Berlin, GERMANY, 2011, pp. 51–59.
[54] M. Hirata, C. Arimoto, N. Hattori, H. Anzai, Can cattle visually discriminate between green and dead forages at a short distance while moving in the field? Anim. Cognit. 22 (5) (2019) 707–718.
[55] M. Hirata, N. Kusatake, How cattle discriminate between green and dead forages accessible by head and neck movements by means of senses: reliance on vision varies with the distance to the forages, Anim. Cognit. 23 (2) (2020) 405–414.